POLITECNICO DI TORINO
Repository ISTITUZIONALE

Assembling and Using a Cellular Dataset for Mobile Network Analysis and Planning

Original
Assembling and Using a Cellular Dataset for Mobile Network Analysis and Planning / Di Francesco, P., Malandrino, F., Dasilva, L.. - In: IEEE TRANSACTIONS ON BIG DATA. - ISSN 2332-7790. - ELETTRONICO. - 99(2018), pp. 1-1. [10.1109/TBDATA.2017.2734100]

Availability:
This version is available at: 11583/2704102 since: 2018-03-27T14:13:01Z

Publisher:
IEEE

Published
DOI:10.1109/TBDATA.2017.2734100

Terms of use:

This article is made available under terms and conditions as specified in the corresponding bibliographic description in the repository

Publisher copyright
IEEE postprint/Author's Accepted Manuscript

©2018 IEEE. Personal use of this material is permitted. Permission from IEEE must be obtained for all other uses, in any current or future media, including reprinting/republishing this material for advertising or promotional purposes, creating new collecting works, for resale or lists, or reuse of any copyrighted component of this work in other works.

(Article begins on next page)

13 June 2026

Design of Isogrid Shells for Venus Surface Probes

Enrico Ossola[1]
Politecnico di Torino, Torino, 10129, Italy
Jet Propulsion Laboratory, California Institute of Technology, Pasadena, California

John Paul Borgonia[2], Morgan Hendry[3], Eric Sunada[4]
Jet Propulsion Laboratory, California Institute of Technology, Pasadena, California

Eugenio Brusa[5] and Raffaella Sesana[6]
Politecnico di Torino, Torino, 10129, Italy

Venus' harsh environment poses a significant challenge for the design of lightweight surface probes. The authors investigated isogrid stiffened spherical shells produced by Additive Manufacturing. A Ti6Al4V, 1.12 m diameter lightweight structural shell capable of surviving a Venus surface environment was designed and assessed via analytical methods and Finite Element Modeling. Sub-scale components (200 mm diameter) were designed, analyzed, fabricated using Laser Powder Bed Fusion and tested under hydrostatic external pressure at ambient temperatures for model validation. A sub-scale sphere was successfully tested under Venus-like pressures and temperatures at a Hot Isostatic Press facility. It was found that additively manufactured isogrid shells could lead to significant mass, cost, and schedule savings, freeing resources for increased science return from future missions.

Nomenclature

b = *Rib Thickness (mm)*

d = *Rib height (mm)*

E = *Young's Modulus (MPa)*

---

[1] PhD student, Department of Mechanical and Aerospace Engineering, Politecnico di Torino, JPL Affiliate.
[2] Group Supervisor, Additive Manufacturing CTR & Sheet Metal Fabrication, Jet Propulsion Lab, Pasadena California
[3] Mechanical Engineer, Mechanical Systems and Technology Group, Jet Propulsion Lab, Pasadena California (AIAA Senior Member)
[4] Principal Engineer, Propulsion, Thermal, and Material Systems Group, Jet Propulsion Lab, Pasadena California
[5] Professor, Department of Mechanical and Aerospace Engineering, Corso Duca degli Abruzzi, 24.
[6] Associate Professor, Department of Mechanical and Aerospace Engineering, Corso Duca degli Abruzzi, 24.
Copyright: © 2020. All rights reserved.

h = *Isogrid triangle height (mm)*

KF = *Knockdown Factor*

m = *Mass (kg)*

p = *Pressure (MPa)*

R = *Radius (mm)*

SF = *Safety Factor*

t = *Skin thickness (mm)*

α, β, δ = *Geometric parameters*

λ = *Buckling Load Factor*

ν = *Poisson's ratio*

ρ = *Density (kg/mm^3)*

σ = *Stress (MPa), Von Mises if not specified*

Subscripts

analyt = *Analytical*

cr = *Critical*

exp = *Experimental*

GI = *General Instability*

LFEA = *Linear Finite Element Analysis*

NL = *Non-Linear Finite Element Analysis*

RC = *Rib Crippling*

SB = *Skin Buckling*

I. Introduction

THE exploration of Venus commenced in 1962 with the flyby of Mariner 2. It was followed by a series of flybys, orbiters, and landers, including Mariner, Venera, Pioneer Venus, Vega, and Magellan missions, which characterized both the overall topography of the planet and the geology specific to the landing sites [1]. Despite nearly 60 years of exploration, many scientific questions about the "Earth's Twin" are still unsolved. As a result, Venus exploration has been identified by NASA as a priority topic [2]. The 2013 Decadal Survey specified a New Frontiers class Venus in-situ mission as one of the top priorities of the science community. Further exploration of Venus could lead to a better understanding of the origin and the evolution of the Earth, other terrestrial planets, and exoplanets. Additionally, with climate change becoming a more pressing issue in our time, understanding an analog atmosphere could help scientists identify better ways to address this issue [3]. A landed mission has been targeted as a mid-term goal, with proposed payloads including instruments to study surface chemistry, mineralogy, or seismology [4]. While the desire for additional missions has long been present in the planetary science community (and many studies funded), the surface environment poses technical challenges that persist to this day.

Venus represents one of the most challenging environments for planetary exploration. The surface of the planet is masked by a thick layer of carbon dioxide gas with sulfuric acid clouds and haze at approximately 25-75 km in altitude. Above the clouds, high speed winds blow at approximately 360 km/h, slowing down to few km/h on the surface where the density is about 67 kg/m^3. At the surface, the pressure and temperature rise to 93 bar and 462 °C, respectively[1,5]. These factors pose a significant challenge for the design of planetary probes, and the maximum surface lifetime achieved by any mission was 127 minutes by Venera 13 in 1978. Every Venus surface mission has utilized a thick, spherical external pressure vessel. This pressure vessel dominates the mass budget of these missions, and poses significant challenges for spacecraft design, integration, and test. While new missions have been proposed, lightweight spherical shells have proved elusive, and the majority of proposers have fallen back to solid titanium.

In order to address this need, several new concepts have been proposed. A concentric sphere layout was used by Hall et al. [6] to design a concept for a Venus deep atmosphere instrument enclosure. The prototype, composed by an outer sphere made of Ti-6Al-4V, an annulus of microfiber felt for thermal insulation and a stainless-steel inner sphere, was fabricated and tested under Venus-like conditions. Bugby et al. [7] suggested a new lightweight vessel, consisting of a two-shell system in which the payload is contained in an internal Polymer Matrix Composite tank. This, in turn, is surrounded by an insulation annulus, pressurized to 100 bar, and contained by an external Titanium shell that can

be made thinner compared to a design for an external buckling pressure. The inner shell, although under a buckling pressure, results in an overall mass savings because it is no longer exposed to the Venus atmosphere, allowing it to be constructed of lightweight Polymer Matrix Composite. However, the two-shell system, high pressure tank, and the required fill and distribution plumbing results in a significant internal volume penalty, robbing the mission of valuable space for scientific payloads. As such, a passive, lightweight structural system that has a more favorable equipment volume/mass ratio is desirable by mission architects. The amount of time prior to reaching maximum equipment temperatures is also a consideration that must be included in an overall mass assessment. The design by Bugby et al. incorporated a water-based expendable coolant within the volume between the two shells. Similar expendable coolant concepts exist for passive structural systems.

In 2006, an assessment of Venusian structural shell materials and fabrication techniques was conducted [8]. Ti-6Al-4V was selected as a promising material for these external pressure vessels due to its low thermal conductivity and good creep/tensile performance at temperature. At that time, only a few standard fabrication techniques were considered, namely spin forming and welding. In recent years, metal additive manufacturing has created new opportunities for new spacecraft structural geometries with existing structural materials, including Titanium [9]. Given demonstrated savings in cost, mass, and schedule on other additive projects [10], this study investigates the potential of this new manufacturing technique to enable new. highly efficient geometries, specifically the use of an internal isogrid.

Isogrids were standardized in the aerospace industry in the 1960s and became a critical structural design technique on missions like Skylab and launch vehicles like the Delta and Atlas [11]. Isogrids represent a trivial 2-D manufacturing problem. On singly curved panels (like cylinders), flat panels can be machined and bent to shape. Unfortunately, this technique becomes either more challenging or more expensive to implement when the surface is doubly curved. A spherical shell with an internal isogrid represents a complex, multi-axial machining problem. For subtractive fabrication of a typical Venus external pressure vessel, a large and expensive hemispherical billet would be required to form the basis of the part. For smaller shells, standard 5-axis machining might prove difficult due to tool geometry limitations. Additive Manufacturing (AM) represents a workaround for fabricating this, and more complex, geometries on almost any scale of interest. Additionally, by switching to an additive process, additional integral features can be added, including (but not limited to) thermal isolators, expendable coolant channels, dampers, shock mitigation, and impact attenuation features.

This study was broken into several phases. First, a conceptual design for a ~1.12 m spherical shell was created and analyzed to bounding Venus surface conditions. Next, to enable testing within today's additive manufacturing capabilities, a 1/5th scale version of the shell was designed and sized to fit on common additive print beds. Using this smaller shell's predicted critical pressure at ambient temperatures, a test campaign was designed to slowly externally load the shell to failure. For comparison, an additively manufactured non-isogrid version of the same shell size was also tested. Using the empirical results and the validated model, the mass savings of a 1.12 m flight shell were estimated. Finally, a test of the 1/5th scale shell was conducted under Venus surface temperatures and pressures at a Hot Isostatic Press (HIP) facility.

Through this work, the authors have shown that AM technology can significantly reduce the cost, fabrication time and mass of planetary atmospheric and surface probes. Furthermore, AM enables multifunctionality. This creates new opportunities for fabricating integrated thermomechanical devices. When taken with the predicted mass reduction, this new shell concept could allow missions to allocate more mass for thermal systems, potentially enabling longer Venus surface lifetimes, increased science return, and human-in-the-loop operations.

While this additively manufactured external pressure vessel technology was proposed for Venus, it could easily be ported to other missions requested in the 2013 Decadal Survey. Jupiter, Uranus, and Neptune deep atmospheric probes and Titan sub ocean probes are examples of other attractive applications (albeit without the harsh high temperature environment). Melt probes designed to burrow into the ice crust of Europa and Enceladus could also benefit from this AM thermal-structural sphere development, specifically in the realm of highly optimized heat exchanger designs for the probe's nose. Finally, proposed Mars Sample Return Containment Vessels and Earth Entry Vehicles could utilize this technology to provide lightweight, crush resistant structures and tunable impact attenuation.

II.External Pressure Vessel Design

A. Problem statement

The concept proposed is a ~1.12 m diameter, Ti-6Al-4V alloy spherical probe with internal isogrid stiffeners for future flight implementation. Inside the isogrid pockets, fluid passages and porous metal wicks would be co-printed with the shell. A manufacturing demo of a spherical cap is shown in Fig. 1, in which a porous wick has been co-printed

in the triangular pockets formed by full-dense skin and ribs. Afterwards, the two individual hemispheres would be integrated together with a compressive seal between them. The thermal design must manage the total energy such that the internal equipment temperature does not exceed 70 °C for up to 24 hours. The cooling system (see schematic in Fig. 2) consists of an evaporation system at the equipment base plate. The vapor/gas mixture then flows through channels incorporated within the structural shell to intercept, via sensible heat, loads coming through from the environment prior to being expended in the Venusian atmosphere through a vent port. As a result, the thermal energy is transferred and released into the Venus environment, and internal heating of the probe is mitigated for a period of time. When combined with phase change materials and passive thermal isolation strategies, it is envisioned that the surface lifetime could be extended significantly. A two-phase mechanically pumped fluid loop thermal control system is currently under development at the Jet Propulsion Laboratory [12] and a concept for a cooling system for a Venus lander has been proposed by Lee and Tarau in [13].

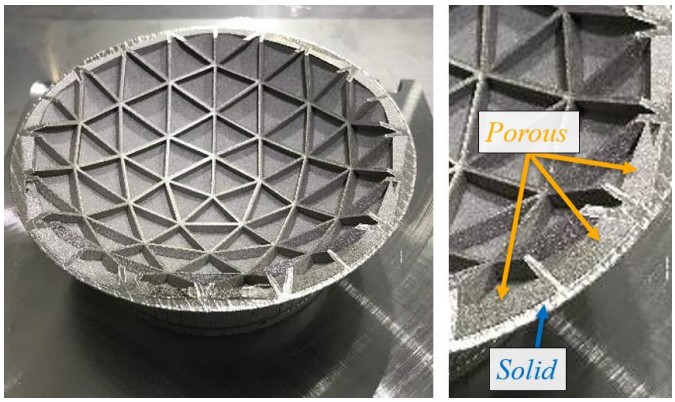

Fig. 1 Manufacturing demo: additively manufactured isogrid-stiffened spherical cap, with co-printed porous wick

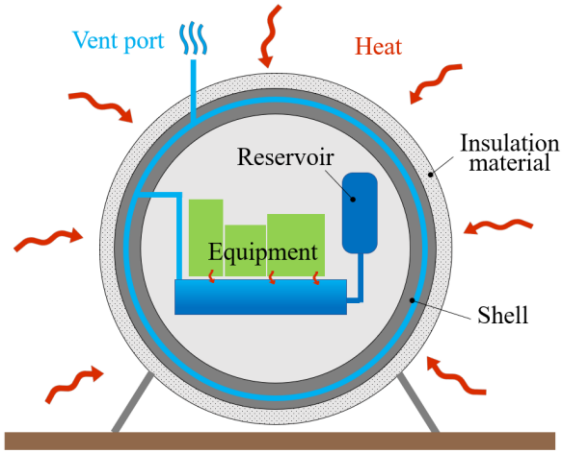

Fig. 2 Concept of a thermal control system

In order to demonstrate the suitability of an additively manufactured isogrid shell for the Venus surface environment, analytical and numerical models were adopted for the preliminary design, and experimental testing for the model validation. In this work, only the structural problem will be addressed, without including any integrated thermal control system. In particular, the shell was designed and analyzed at full scale. Once an optimized design was finalized, subscale versions of both isogrid and non-isogrid shells were modeled and fabricated using additive processes. These were tested in a relevant pressure environment at ambient temperature to validate the modeling techniques.

B. Mechanical Requirements

The pressure vessel is subjected to multiple loading conditions, corresponding to different phases of the mission (launch, cruise, and landing within the Venus environment). In the early design stage, only the pressure loads of Venus' atmosphere were considered. Landing loads were assumed to be negligible compared to the pressure load, as it was expected that they can be limited by utilizing crushable energy absorbers in the lander legs [14].

Two failure modes are connected to an external pressure loading: 1) yielding and 2) instability of the elastic equilibrium. Yielding can be accurately predicted by using analytical or numerical analysis. By the contrast, elastic instability (or buckling) can be harder to predict. As material and geometry imperfections cause high discrepancies between predicted and experimental results, an empirical Knockdown Factor (*KF*) is usually applied to the results of

a linear buckling analysis. *KF* values are obtained by experimental activities and vary depending on geometry, size, boundary conditions, materials, and geometric imperfections. As the thermal control system and, consequently, the temperature of the shell have not been defined, the design pressure and the safety factors used for the yielding and buckling analyses have been conservatively selected as 100 bar and 1.5, respectively. This is greater than the mean atmospheric pressure at the surface of the planet (93 bar), and greater than the typical safety factor for NASA structural design [15]. This allowed the analysis to account for the degradation of the material properties with temperature, such as a reduction of Young's modulus and Yield strength (up to 25% when the temperature is increased to 350°C [16–18]) . In the case of an actual mission, these properties will be defined by the project with an eye towards assuming an acceptable level of risk. Lower safety factors (SF_{yield} = 1.25, $SF_{ultimate}$ = 1.4), together with material properties at the expected temperature can be applied, if specific testing activities are performed (according to NASA standard structural design practices) [15].

C. Structural shell design: Plain Sphere

Past missions to Venus adopted thick, unstiffened spherical pressure vessels, composed of two or three flanged segments [5,19]. Well known analytical formulas for stress and buckling analysis for simply supported thin spherical shells subjected to external pressure are reported below, in the spherical coordinate system (r, θ, φ), where p is the external pressure, R and t are the sphere radius and the shell thickness and E and ν are the Young's modulus and the Poisson's ratio of the material. Equation 2, commonly referred as the Zoelly's buckling equation [20–23], describes the elastic buckling critical pressure for thin spherical shells undergoing uniform external pressure. This equation has to be corrected by adopting the knockdown factor *KF*, whose recommended values could vary from 14% (NASA Technical Report [24]) to 30% (industrial application, according to [25]). A summary of past experimental works about KF was given by Lee [26], Evkin [27] and Wagner [28], who conducted analytical, numerical and experimental investigations aimed to better predict the buckling behavior of spherical shells and to provide improved design factors

.

$$\begin{cases} \sigma_r = 0 \\ \sigma_\theta = \sigma_\phi = \dfrac{pR}{2t} \end{cases} \tag{1}$$

$$p_{cr} = \frac{2E}{\sqrt{3(1-\nu^2)}} \frac{t^2}{R^2} \tag{2}$$

$$p_{cr}^{exp} = KF\, p_{cr} \tag{3}$$

Similarly, Finite Element Analysis (FEA) can be used. The linear bifurcation analysis predicts the critical pressure, by solving the related eigen-value problem. It has been found that the FEA results are in accordance with Zoelly's formula for unitary *KF*. As reported by Rotter [29] and by the European Standard Code [30], more sophisticated tools involve non-linear analyses, including material non-linearity, geometric non-linearity and simulation of typical imperfections.

D. Structural shell design: Isogrid

1. Analytical formulas

Isogrid structures are composed of a skin (planar, single curved or doubled curved), and a number of ribs (usually with a rectangular or H-shaped section). These ribs form triangular cells projecting from the skin surface. The name isogrid is related to their macroscopic mechanical behavior: due to the equilateral triangles, this structure acts mainly as an isotropic material. The main literature references about spherical isogrid structures are Bellifante and Meyer [31] and the "NASA Isogrid Design Handbook" [11]. Isogrid spherical structures can be obtained from an inscribed icosahedron, dividing its faces in smaller triangles and projecting them on the sphere, so that the size of the triangles is a function of the radius of the sphere and the number of subdivisions (also known as "isogrid density"). The main design parameters are shown in the cross section reported in Fig. 3.

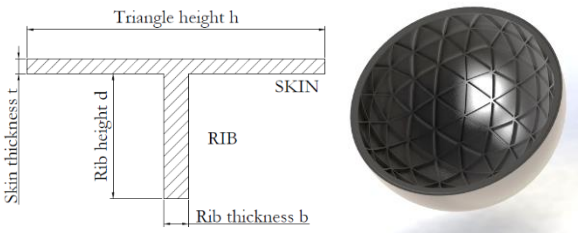

Fig. 3 Isogrid cross section and Isogrid sphere

As described in [11], the stress state of isogrid spherical shells can be described as a function of the following non-dimensional geometrical parameters:

$$\alpha = \frac{bd}{th}$$
$$\delta = \frac{d}{t} \tag{4}$$
$$\beta = \sqrt{3\alpha(1+\delta)^2 + (1+\alpha)(1+\alpha\delta^2)}$$

where b, d, t and h are the rib thickness, the rib height, the skin thickness and the triangle height respectively, as shown in Fig. 3.

The principal stresses in the skin and ribs are calculated as follows, according to [11] :

$$\sigma_{\theta,\phi}^{skin} = \frac{pR}{2t(1+\alpha)}$$
$$\sigma_1^{rib} = \frac{pR}{3t(1+\alpha)} \tag{5}$$

Three buckling modes can occur: General Instability (GI) of the whole structure, Skin Buckling (SB) on the shell of the triangular cells, or Rib Crippling (RC), as shown in Fig. 4. As reported in [11], the GI equation derives from the Zoelly's formula for the perfect sphere, modified in order to take into consideration the contribution of the ribs. The SB equation is the buckling critical load of a planar triangle hinged on the edges and subjected to a compressive in-plane load normally to the edges. Finally, the RC equation considers rectangular plates (the curvature is neglected), hinged on 3 edges and loaded on the two opposite short edges.

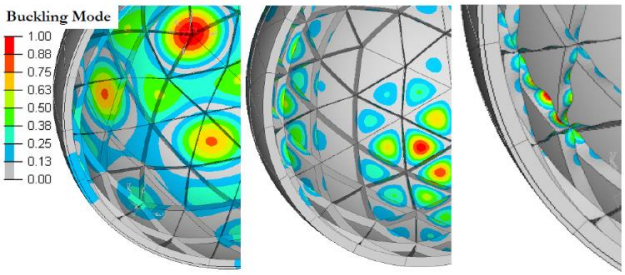

Fig. 4 Buckling modes: General Instability (left), Skin Buckling (center) and Rib Crippling (right)

$$p_{GI} = c_0 2E\frac{t^2}{R^2}\beta, \qquad c_0 = 0.26$$
$$p_{SB} = c_1 2E\frac{t(1+\alpha)}{R}\frac{t^2}{h^2}, \qquad c_1 = 3.47 \tag{6}$$
$$p_{RC} = c_2 2E\frac{t(1+\alpha)}{R}\frac{b^2}{d^2}, \qquad c_2 = 0.634$$

The GI equation is obtained from the buckling formula for plain shells (Eq. 2 and 3), where c_0 is calculated as:

$$c_0 = \frac{KF}{\sqrt{3(1-\nu^2)}} \tag{7}$$

According to [11], the empirical parameter c_0 is equal to 0.26 (corresponding to a *KF* of 42.9%). This value is derived from the experimental activities reported in [31], where 3 plastic domes and 1 Aluminum dome were tested.

2. Isogrid optimization

The optimization portion of this study sought to identify the configuration (*h, t, b* and *d*) of minimum mass, which satisfies the stress and critical buckling pressure requirements. Starting from [11], an optimization procedure is proposed: the simultaneous failure mode design was adopted, assuming that the optimal configuration is the one for which the three buckling modes take place at the same time. This design criteria, although not always applicable, was found to be effective in this case.

Having defined the buckling load factor as $\lambda = {}^{p_{cr}}/_{p}$, the optimum structure is the one for which all the three modes of buckling take place at the same time:

$$\lambda_{GI} = \lambda_{SB} = \lambda_{RC} \Rightarrow optimum\ layout \tag{8}$$

In the proposed optimization code, the triangle height *h* is an input datum. It must be noted that, given the sphere radius, *h* can vary discretely only, as it depends on the isogrid frequency, i.e. the number of subdivisions of the original icosahedron, which is an integer. Running the code multiple times, it is possible to find the optimum isogrid frequency. As such, the design variables are reduced to three parameters only (*t, b* and *d*). Considering the system of the SB and RC equations, one can find the rib height as function of skin and rib thickness for which Skin Buckling and Rib Crippling occur at the same pressure load:

$$d = \frac{bt}{h}\sqrt{\frac{c_2}{c_1}} \Rightarrow \lambda_{SB} = \lambda_{RC} \tag{9}$$

Given the baseline shell geometry, the isogrid frequency, material properties, and the external load, the failure modes were plotted as functions of skin thickness and rib thickness. The optimum curve was obtained by the intersection of these three failure modes, as shown by Fig. 5. Given the required buckling load factor λ, the optimum configuration for the isogrid shell is fully determined. All isogrid geometric features, as well as iso-curves of mass,

can be easily read by projecting the plot on the *b-t* plane, as shown by Fig. 7. Finally, maximum stress was to be verified.

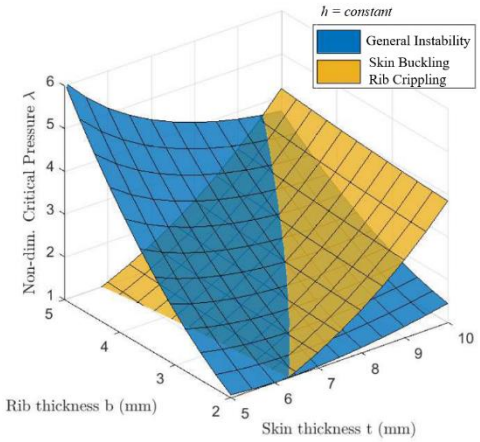

Fig. 5 Intersection between the buckling modes for different values of skin and rib thickness

3. Finite Element Analysis

Finite Element Analysis (FEA) was performed using MATLAB and HyperMesh as preprocessors and OptiStruct as the solver. The hemisphere was modeled using quadrangular shell elements (approx. 150000 nodes), as shown in Fig. 6. Linear static analysis and linear buckling analysis were performed. Displacement and stresses predicted by FEA were found to be in agreement with the analytical model previously described. By the contrast, discrepancies in the predicted buckling critical pressure were observed. Indeed, the analytical formulation contains a knockdown factor (c_0), experimentally derived. The Finite Element (FE) linear buckling analysis, on the contrary, doesn't take into consideration the effects of imperfections, intrinsically present in actual components, thus overestimating the buckling resistance of spherical shells, as described in the previous sections about plain shells. Moreover, it has to be noticed that the sensitivity to imperfections is not constant, as it can vary from plain to stiffened shells, as suggested by the experimental activities described in [31]. For this reason, FEA optimization tools, such as topology or size optimization, were found to be not effective when used with the linear analyses. In order to predict the actual critical pressure, non linear simulations should be performed instead, including material and geometric non linearities [21,22]. However, the very high computational cost makes these simulations not well suited for topology optimization loops. For this reason, it was decided to adopt the analytical formulation previously described to design and optimize the structure, while using FEA only in a second step, to check the mechanical behavior of the optimized structure.

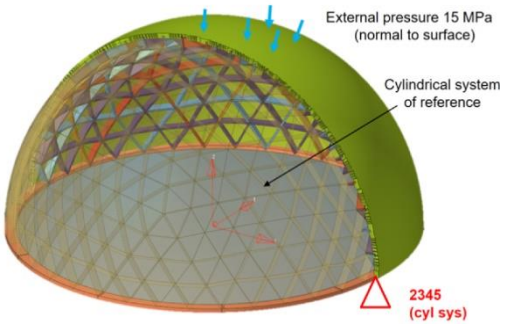

Fig. 6 Finite Element Model

III.Venus probe structural shell design

A. Full scale model

The analytical formulations previously reported were used to make a preliminary design of the Venus pressure vessel (Ti6Al4V, R=560mm). A plain shell and two isogrid shells were designed, having different isogrid frequencies (*h*=157 and 79 mm). As an example, the optimization plot for *h*=157 is reported in Fig. 7. This plot can be seen as the top view of Fig. 5, in which the yellow curve represents the intersection between the three buckling modes, the black lines show the rib height, the red curves are the iso-mass curves and the blue ones are the iso-λ curves (i.e. the non dimensional critical pressure). The design point was obtained by intersecting the yellow curve with the required critical pressure. All configurations were designed to have $\lambda^{FEA} = {p_{cr}^{FEA}}/{p} = 3.2$. In the case of a plain sphere, this corresponds to *KF*=30% approximately, as suggested by Roark's [25]. Table 1 summarizes the results, comparing the plain layout to two isogrid layouts, with h=157 and 79 mm. It was found that, considering the same required λ for both plain and isogrid: 1) all three configurations lead to approximately the same mass, 2) isogrid configurations exhibit higher stresses, 3) among the isogrid shells, *h*=157 mm is the best (lower stresses, see FEA results in Fig. 8). This *h* value will be considered for the further analyses. It must be noted that *KF*s for plain and isogrid shells could be significantly different and, consequently the required λ value could differ as well. For this reason, subscale components were designed, fabricated and tested.

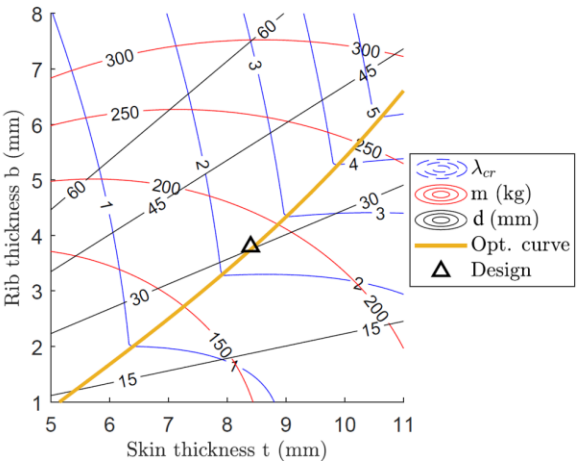

Fig. 7 Optimum geometry (for *h*=157 mm)

Table 1 Full-scale shell: geometric parameters and main results

		Plain	Isogrid (A)	Isogrid (B)
h	mm	-	157	79
t	mm	10.5	8.4	5
d	mm	-	30	30
b	mm	-	3.8	4.5
m sphere	kg	182	184	179
σ_{analyt}	MPa	400	460	625
λ_{analyt}	-	3.20	2.43	2.54
σ_{LFEA}	MPa	400	469	695
λ_{LFEA}	-	3.20	3.20	3.22

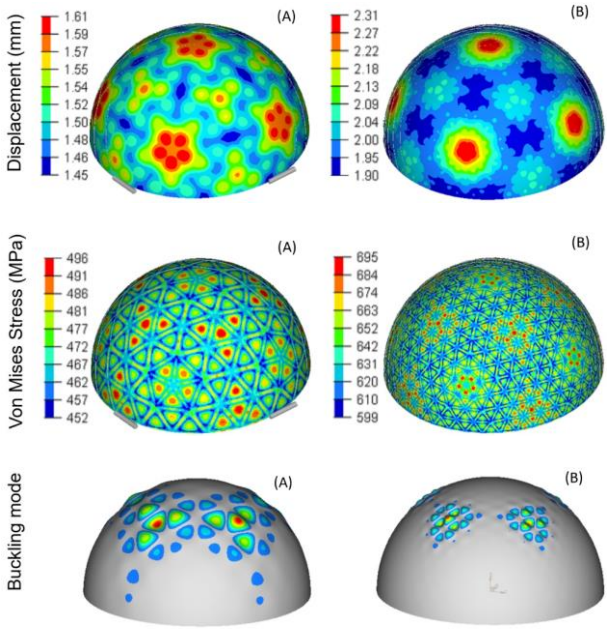

Fig. 8 FEA results: displacement, Von Mises Stress and first buckling mode for Isogrid A (left column) and B (right column) configurations

B. Redesign for 1/5th scale

The experimental activities described in the following sections were aimed to assess the actual failure pressure and validate the predictive models. A 1/5th scale was designed, fabricated, and tested. This scale was selected due to LPBF print bed limitations. The minimum feature size was set to 1 mm, due to the limits of today's additive manufacturing processes. Shell features were designed according to the design procedure previously described; this resulted in a critical pressure for each hemisphere well above Venus surface pressure at ambient temperature.

Isogrid and non-isogrid R=100 mm spheres were designed, according to the plot reported in Fig. 9. Similarly to Fig. 7, the curve of the optimum design was mapped as a function of the main isogrid parameters. The design space was reduced, to take into account the limitations due to manufacturability issues. Then, the isogrid model was modified, adding chamfers and fillets, in order to improve manufacturability. Non-linear analyses were performed on two different models, using shell or solid elements respectively. In the latter case (Fig. 10), symmetric boundary conditions were used and only 1/5th of the component was modeled, in order to reduce the computational cost. Design details are reported in Table 2. The failure pressure calculated by the non-linear models was considerably different from the predictions made by the linear models when a *KF* of 30% was applied. One additional non-linear simulation

was performed on the isogrid solid element model, considering material properties at 500 °C (Venus environment). The predicted failure pressure was 198 bar. The results of these simulations will be used in the following activities (see Section V – Testing).

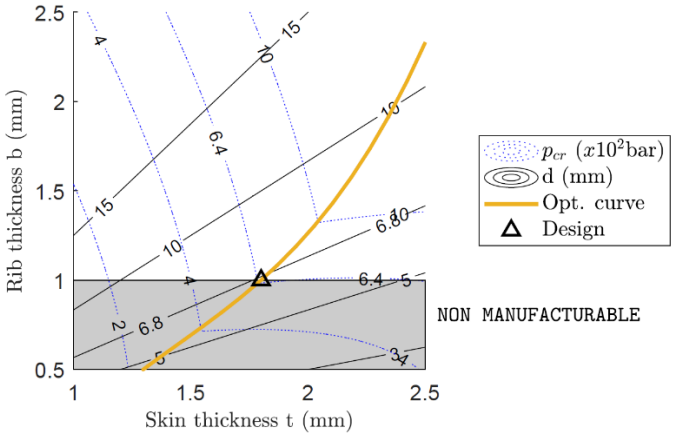

Fig. 9 Scaled model: isogrid optimum geometry

Table 2 Scaled model: comparison between plain and isogrid models

		Plain	Isogrid	Isogrid modified
h	mm	-	28	28
t	mm	2.7	1.8	1.8
d	mm	-	6.8	6.8
b	mm	-	1	1
m hemisphere (without flange)	kg	0.731	0.690	0.833
Analytical				
p_{cr}^{analyt}	bar	971	640	NA
Linear FEA				
σ (100 bar)	MPa	185	269	251
p_{cr}^{LFEA}	bar	971	810	934
30% p_{cr}^{LFEA}		291	243	280
Non-Linear FEA				
p_{cr}^{NL-2D}	bar	448		507
p_{cr}^{NL-3D}	bar	523		510

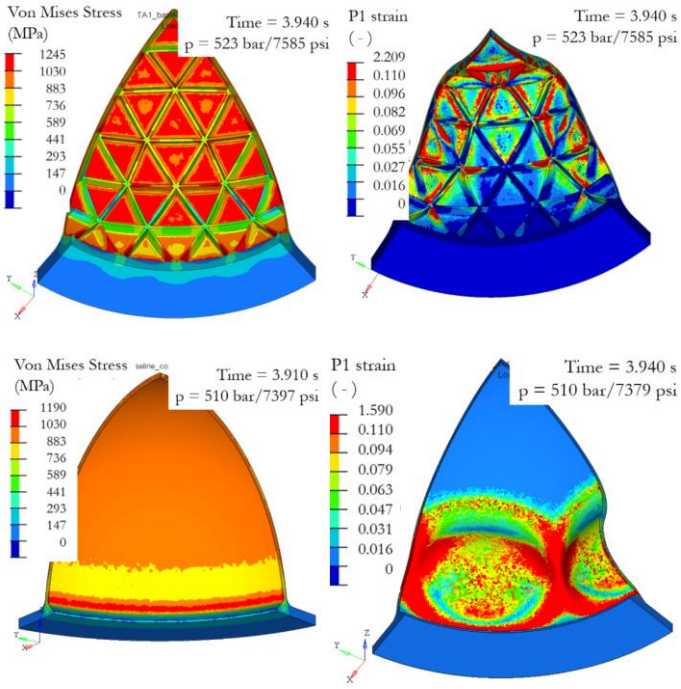

Fig. 10 Non-linear analysis - solid element scaled model

IV. Manufacturing

Laser Powder Bed Fusion (LPBF) was chosen for additive manufacturing as it allows for process parameter adjustment, which can control the density of a part. This enables LPBF to 3D print a part with both porous and fully dense sections in the same manufacturing build. This enables integrated thermal control systems, such as evaporators with porous wicks [32]. If those features are not required, other Ti-6Al-4V additive manufacturing techniques are available.

Eight 1/5th scale shells were 3D printed and finished machined to remove support material and improve surface finish for all mating interfaces. All shells exhibited manufacturing defects in the shape of a 50-70 mm long line, located on the external surface of the shell (Fig. 11). These defects may have been attributed to thermal stress in the LPBF process and titanium's low thermal conductivity. Typical AM Ti-6AL-4V parts undergo stress relief, HIP, and then solution treatment. Due to time constrains and testing schedules, solution treatment was omitted.

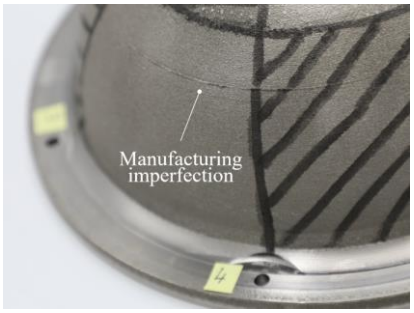

Fig. 11 Manufacturing imperfection. A system of reference was marked on the shells, to help in locating the failures.

A production cost and a schedule analysis (Table 3) was done to compare AM versus traditional subtractive manufacturing, according to a quotation from an external vendor. The quotes are referred to 7 isogrid hemispheres and 1 plain hemisphere, with machined flanges; costs may vary depending on the production lot size. With AM, very little material removal is required, whereas full subtractive machining will require fabricating the isogrid shells from titanium billets using Computer Numerical Control (CNC) mills and lathes. AM provided a cost and schedule savings of 26% and 79% respectively in producing the structural shells at this scale.

Table 3 Cost and schedule comparison

Traditional manufacturing	
Material: 8 round billets	$ 19840
Non-recurring engineering costs	$ 10200
Machining (7 isogrid shells)	$ 48485
Machining (1 plain shell)	$ 17480
Total cost	**$ 96005**
Total lead time	**42 weeks**
Additive manufacturing	
Fabrication (7 isogrid + 1 plain)	$ 49890
Finish machining	$ 21000
Total cost	**$ 70890**
Total lead time	**9 weeks**

V.Testing

A. Model Validation

The model validation test was conducted by submerging a hemispherical shell with a thick backing plate in a hydrostatic chamber filled with water, as shown in Fig. 12. The hemisphere was filled with plastic beads to mitigate the pressure wave during implosion. While monitoring the shell via a live video, pressure was increased from ambient to failure. One non-isogrid shell and three isogrid shells were tested. The non-isogrid shell collapsed at 317 bar. The three isogrid hemispheres failed at 410.3 ± 4.0 bar (414, 411, 406 bar). In all cases, the failure consisted in a sudden and violent implosion of the shell. Based on the recordings and on the location of the failure (see supplementary material), it is believed that the failure event started near and propagated from the largest manufacturing imperfection on each part. Fig. 13 shows the components after testing; plastic beads are visible, stuck on the internal surface as a consequence of the violent pressure wave. Experimental results are summarized and compared to predictions in Table 4.

Several results were observed. First, the failure mode for the isogrid hemispheres was consistent from test article to test article and the dispersion of the failure pressure was very low as well. Second, the *KF* of the AM plain sphere is accordance to the values suggested by Roark's in [25]. Third, the *KF* of the isogrid sphere is higher than the non-isogrid design. Fourth, in the case of the isogrid shells, the difference between the failure pressure predicted by the non-linear simulations and the experimental results is less than 10%. In the case of the plain shell, by the contrast, a larger difference is observed (60%). It must be noticed that the simulations were performed considering a perfect hemisphere, but manufacturing defects were observed in the components before testing. The large difference between predictions and experimental results in the plain shell can probably be related to this, as imperfections and defects can trigger shell instability, significantly reducing the load capacity [26]. Moreover, it is worth noticing that the failure mode of the isogrid shells observed during testing was not clearly buckling or yielding. However, the high stresses predicted by the linear FEA suggest that the shells may have collapsed because of yielding.

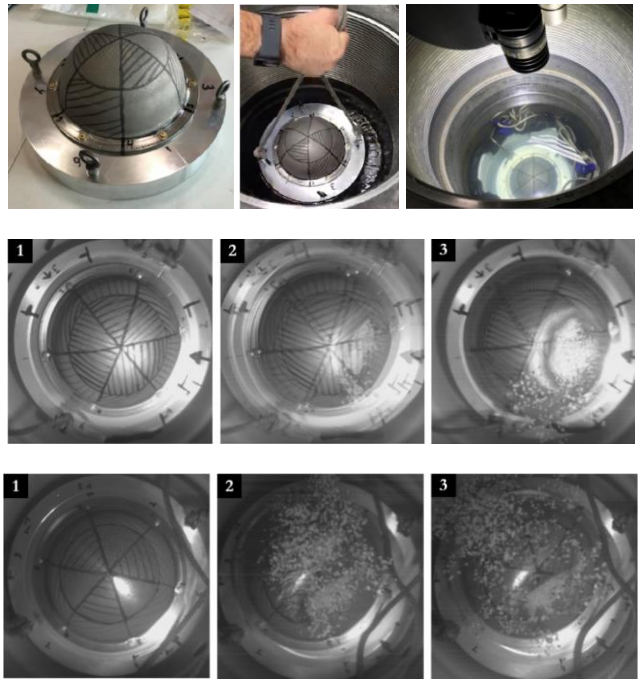

Fig. 12 Hydrostatic test: test setup, collapse of plain-SN00 and iso-SN05 hemisphere

Fig. 13 Tested components: plain-SN00 (first column), isoSN01 (second column), iso-SN04 (third column), iso-SN05 (fourth column).

Table 4 Experimental results vs predictions

		Plain	Isogrid
p_{cr}^{exp}	bar	317	410
p_{cr}^{LFEA}	bar	917	934
$KF = p_{cr}^{exp}/p_{cr}^{LFEA}$		33%	44%
p_{cr}^{NL-2D}	bar	507	448
$p_{cr}^{NL-2D} vs\ p_{cr}^{exp}$		+60%	+9%

B. Relative Environment Test

The relative environment test was conducted by placing a fully assembled sphere in a Hot Isostatic Press (HIP) chamber. The sphere was filled with ceramic beads to mitigate a pressure wave in the event of a violent failure. Pressure and temperature of the HIP chamber were increased until they reached 98 bar ±7 bar at 494 °C ± 14 °C. Then, the chamber conditions were held for 1 hour (+15/-0 minutes). After one hour, the pressure and temperature of the HIP chamber were slowly returned to ambient. According to the non-linear analyses performed considering the material properties at 500°C, no failure was expected, with a Factor of Safety of approximately 2:

$$FS = \frac{p_{fail}^{FEA}}{p_{test}} = \frac{198\ bar}{98\ bar} \approx 2 \tag{10}$$

The sphere survived this environment, showing no signs of damage from the temperature and pressure. Oxidation of the internal surfaces was noted, most likely due to the chemical reaction with moisture or coating of the beads (Fig. 14).

Fig. 14 Component after relevant environment testing: external and internal surfaces.

VI. Re-design of the full-scale model

The full-scale model was re-designed utilizing what was learned from the sub-scale experimental campaign, considering the results of the experimental activities performed on the sub-scale components. The analytical model

was used to obtain the optimal isogrid configuration (Table 5), considering a design pressure of 150 bar and a KF equal to 44%, i.e. assuming the same KF as the tested sub-scale components. In fact, as reported by [23,24], KF depends on the radius to thickness ration (R/t), which was found to be similar in both the sub-scale and full-scale components. Further testing should be conducted to verify the validity of this assumption. As a result, the isogrid component was found to be 14% lighter than the plain shell.

Table 5 Redesign of the Full-scale shell

		Plain	Isogrid (Updated)
KF		30%	44%
h	mm	-	157
t	mm	10.5	7.5
d	mm	-	26
b	mm	-	2.9
m sphere	kg	182	156
σ_{LFEA}	MPa	400	560

VII.Conclusion

Most of the designs of Venus surface probes consist in spherical pressure vessels, as the spherical shape minimizes the surface area exposed to the Venus' atmosphere, given the internal volume. However, plain spherical shells undergoing external pressure loading are very sensitive to imperfections, which can trigger the shell instability. In this paper isogrid stiffened spherical shells fabricated by Additive Manufacturing have been investigated. An analytical design model has been described and applied to a concept of a Venus lander. AM subscale isogrid shells for high pressure environments have been designed, analyzed, fabricated and tested. Ambient temperature hydrostatic testing provided evidence for model validation. In spite of the presence of manufacturing defects, a good match between non-linear predictions and experimental results was found, contrary to plain shells. Moreover, considering the linear approach, the isogrid shells resulted in more favorable values of buckling *KF*s, higher than the ones recommended by NASA standards or industrial application for plain spheres. The tested isogrid shells appeared to collapse via yielding failure in the isogrid ribs, not global buckling. Since a tensile yielding failure is more understood and consistent than

buckling, lower structural margins could potentially be used for an isogrid shell vs. a plain structural shell (per a project's risk posture). This could result in further mass savings after optimization.

. The results of the experimental activities performed on sub-scale components suggested that an isogrid layout could potentially provide up to 14% mass saving, if compared to plain shells. Furthermore, a comparison with traditional subtractive manufacturing showed that AM can provide significant cost (-26%) and mass (-79%) savings. In addition to mass, cost, and schedule savings, it can also provide multi-functionality, allowing complex geometries and integral designs not possible with traditional manufacturing.

Funding Sources

The research described in this publication was carried out at the Jet Propulsion Laboratory, California Institute of Technology, under a contract with the National Aeronautics and Space Administration (NASA).

Acknowledgments

The authors gratefully acknowledge Mahesh Patel for FEA assistance, Ricky Palomares for support equipment design, and DeepSea Power & Light, San Diego, CA and KittyHawk Inc, Garden Grove, CA for the support during the testing activities.

References

[1] Taylor, F. W., Svedhem, H., and Head, J. W. "Venus: The Atmosphere, Climate, Surface, Interior and Near-Space Environment of an Earth-Like Planet." *Space Science Reviews*, Vol. 214, No. 1, 2018. doi:10.1007/s11214-018-0467-8.

[2] Glaze, L. S., Wilson, C. F., Zasova, L. V., Nakamura, M., and Limaye, S. *Future of Venus Research and Exploration*. 2018.

[3] Way, M. J., Del Genio, A. D., Kiang, N. Y., Sohl, L. E., Grinspoon, D. H., Aleinov, I., Kelley, M., and Clune, T. "Was Venus the First Habitable World of Our Solar System?" *Geophysical Research Letters*, Vol. 43, No. 16, 2016, pp. 8376–8383. doi:10.1002/2016GL069790.

[4] VEXAG Venus Exploration Analysis Group. *Roadmap for Venus*. https://www.lpi.usra.edu/vexag/reports/Roadmap-140617.pdf, 2014.

[5] Basilevsky, A. T., and Head, J. W. "The Surface of Venus." *Reports on Progress in Physics*, Vol. 66, No. 10, 2003, pp. 1699–1734. doi:10.1088/0034-4885/66/10/R04.

[6] Hall, J. L., MacNeal, P. D., Salama, M. A., Jones, J. A., and Heun, M. K. "Thermal and Structural Test Results for a Venus Deep-Atmosphere Instrument Enclosure." *Journal of Spacecraft and Rockets*, Vol. 37, No. 1, 2000, pp. 142–144. doi:10.2514/2.3539.

[7] Bugby, D., Seghi, S., Kroliczek, E., Pauken, M., and Robertson, G. A. Novel Architecture for a Long-Life, Lightweight Venus Lander. No. 1103, 2009, pp. 39–50.

[8] Pauken, M., Kolawa, E., Manvi, R., Sokolowski, W., and Lewis, J. Pressure Vessel Technology Developments. 2006.

[9] Brusa, E., Sesana, R., and Ossola, E. "Numerical Modeling and Testing of Mechanical Behavior of AM Titanium Alloy Bracket for Aerospace Applications." *Procedia Structural Integrity*, Vol. 5, 2017, pp. 753–760. doi:10.1016/j.prostr.2017.07.166.

[10] Shapiro, A. A., Borgonia, J. P., Chen, Q. N., Dillon, R. P., McEnerney, B., Polit-Casillas, R., and Soloway, L. "Additive Manufacturing for Aerospace Flight Applications." *Journal of Spacecraft and Rockets*, Vol. 53, No. 5, 2016, pp. 952–959. doi:10.2514/1.A33544.

[11] Meyer, R. R., Harwood, O. P., and Orlando, J. I. "Isogrid Design Handbook." *NASA CR 124075*, 1973.

[12] Furst, B. I., Cappucci, S., Roberts, S. N., Daimaru, T., Sunada, E. T., and Donnell, T. P. O. An Additively Manufactured Evaporator with Integrated Porous Structures for Two-Phase Thermal Control. 2018.

[13] Lee, K., and Tarau, C. 24 Hours Consumable-Based Cooling System for Venus Lander. 2019.

[14] Sly, J. R., Maghsoudi, E., Pauken, M. T., Aubuchon, P. J., Dunkl, J. M., Kochk, J. R., Hyeong, J. L., and Rabinovitch, J. "Dynamic High Temperature and Pressure Characterization of an Inconel Honeycomb Impact Attenuator." *AIAA/ASCE/AHS/ASC Structures, Structural Dynamics, and Materials Conference, 2018*, No. 210049, 2018, pp. 1–45. doi:10.2514/6.2018-1444.

[15] NASA STD 5001B. *Structural Design and Test Factors of Safety for Spaceflight Hardware*. 2016.

[16] Baitimerov, R. M., Lykov, P. A., Radionova, L. V., Akhmedianov, A. M., and Samoilov, S. P. An Investigation of High Temperature Tensile Properties of Selective Laser Melted TI-6AL-4V. 2018.

[17] Popovich, A., Sufiiarov, V., Borisov, E., and Polozov, I. Microstructure and Mechanical Properties of Ti-6AL-4V Manufactured by SLM. 2015.

[18] Zhao, J. R., Hung, F. Y., Lui, T. S., and Wu, Y. L. "The Relationship of Fracture Mechanism between High Temperature Tensile Mechanical Properties and Particle Erosion Resistance of Selective Laser Melting Ti-6al-4v Alloy." *Metals*, 2019. doi:10.3390/met9050501.

[19] Fimmel, R. O., Colin, L., and Burgess, E. "Pioneer Venus." *NASA SP-461*, 1983. doi:.1037//0033-2909.I26.1.78.

[20] Von Karman, T., and Tsien, H.-S. “The Buckling of Spherical Shells by External Pressure.” *Journal of the Aeronautical Sciences*, Vol. 7, No. 2, 1939, pp. 43–50. doi:10.2514/8.1019.

[21] Tall, M., Hariri, S., Le Grognec, P., and Simonet, Y. “Elastoplastic Buckling and Collapse of Spherical Shells under Combined Loadings.” *Thin-Walled Structures*, Vol. 123, No. July 2017, 2018, pp. 114–125. doi:10.1016/j.tws.2017.10.041.

[22] Zhang, J., Zhang, M., Cui, W., Tang, W., Wang, F., and Pan, B. “Elastic-Plastic Buckling of Deep Sea Spherical Pressure Hulls.” *Marine Structures*, Vol. 57, 2018, pp. 38–51. doi:10.1016/j.marstruc.2017.09.007.

[23] Jiménez, F. L., Marthelot, J., Lee, A., Hutchinson, J. W., and Reis, P. M. “Technical Brief: Knockdown Factor for the Buckling of Spherical Shells Containing Large-Amplitude Geometric Defects.” *Journal of Applied Mechanics*, Vol. 84, No. 3, 2017, pp. 1–4. doi:10.1115/1.4035665.

[24] NASA SP 8032. Buckling of Thin-Walled Doubly Curved Shells. 1–33.

[25] Young, W. C., Budynas, R. G., and Sadegh, A. M. *Roark’s Formulas for Stress and Strain*. McGraw-Hill New York, 2002.

[26] Lee, A., Jiménez, F. L., Marthelot, J., Hutchinson, J. W., and Reis, P. M. “The Geometric Role of Precisely Engineered Imperfections on the Critical Buckling Load of Spherical Elastic Shells.” *Journal of Applied Mechanics, Transactions ASME*, Vol. 83, No. 11, 2016, pp. 1–11. doi:10.1115/1.4034431.

[27] Evkin, A. Y., and Lykhachova, O. V. “Energy Barrier as a Criterion for Stability Estimation of Spherical Shell under Uniform External Pressure.” *International Journal of Solids and Structures*, Vol. 118–119, 2017, pp. 14–23. doi:10.1016/j.ijsolstr.2017.04.026.

[28] Wagner, H. N. R., Hühne, C., and Niemann, S. “Robust Knockdown Factors for the Design of Spherical Shells under External Pressure: Development and Validation.” *International Journal of Mechanical Sciences*, Vol. 141, No. January, 2018, pp. 58–77. doi:10.1016/j.ijmecsci.2018.03.029.

[29] Rotter, J. M. “Shell Buckling Design and Assessment and the LBA-MNA Methodology.” *Stahlbau*, 2011. doi:10.1002/stab.201101491.

[30] 1993-1-6, E. *Eurocode 3: Design of Steel Structures: Strength and Stability of Shell Structures*. 2007.

[31] Bellifante, R. J., and Meyer, R. R. *NASA-CR-62257 Fabrication and Experimental Evaluation of Common Domes Having Waffle-like Stiffening*. Santa Monica, CA, United States, 1964.

[32] Daimaru, T., Furst, B., Cappucci, S., Sunada, E., and Birur, G. Development of an Evaporator Using Porous Wick Structure for a Two-Phase Mechanically Pumped Fluid Loop. 2019.